JOURNAL OF Applied Polymer SCIENCE

Production of 3D Scaffolds Applied to Tissue Engineering Using Chitosan Swelling as a Porogenic Agent

Roberta Helena Mendonça,[1,2] Taíla de Oliveira Meiga,[1] Marysilvia Ferreira da Costa,[1] Rossana Mara da Silva Moreira Thiré[1]

[1]PEMM/COPPE, Universidade Federal do Rio de Janeiro, Ilha do Fundão, PO Box 68505, 21941-972, Rio de Janeiro, RJ, Brazil
[2]DEQ/IT, Universidade Federal Rural do Rio de Janeiro, Rod BR 465, 23890-000, Seropédica, RJ, Brazil
Correspondence to: M. F. da Costa (E-mail: marysilvia@metalmat.ufrj.br)

ABSTRACT: The preparation of 3D scaffolds using poly(3-hydroxybutyrate) (PHB) and chitosan (CTS) has been proposed because of the favorable interactions of these materials with mammalian cells in particular osteoblasts (HOB). In this work, a new method of producing porous 3D scaffolds based on the swelling of a dense matrix of PHB and CTS was developed. Scanning electron microscopy images showed the formation of an interconnected porous CTS structure inside a PHB structure. The pore formation was attributed to the swelling of CTS. The scaffolds presented 70% porosity, heterogeneous pore-size distribution, and a compressive modulus equal to (13.07 ± 0.014) MPa, which is close to that of cancellous bone. *In vitro* cytotoxicity assays indicate that the scaffold was not cytotoxic. Its morphology, chemical, and physical properties indicate that the scaffold produced by this new methodology has potential applications in bone-tissue engineering, with drug-delivery capabilities. © 2012 Wiley Periodicals, Inc. J. Appl. Polym. Sci. 129: 614–625, 2013

KEYWORDS: biomaterials; biomedical applications; porous materials

Received 14 April 2012; accepted 14 October 2012; published online 16 November 2012
DOI: 10.1002/app.38735

INTRODUCTION

The development of 3D scaffolds applied to tissue engineering has attracted the interest of various research groups around the world. Many techniques and materials have been studied to produce scaffolds with suitable bulk properties, such as porosity and pore-size distribution.[1–6] In this context, biodegradable polymers have attracted much attention because they can be tailored to degrade within a time frame compatible with tissue growth. Among these materials, the biopolymer poly(3-hydroxybutyrate) (PHB) is of particular interest for bone-tissue engineering since devices made of PHB are compatible with some cultured mammalian cells, including osteoblasts.[7–11] PHB has not been used as a structural material because of its brittleness and narrow "processability window" [i.e., its melting temperature (T_m) is very close to the point of thermal degradation].[12] One of the strategies used to improve its properties is to blend PHB with others polymers, such as chitosan (CTS), a cationic polysaccharide derived from the deacetylation of chitin.[13,4] CTS use is encouraged due to its minimal foreign body reaction and antibacterial nature. Additionally, CTS scaffolds have been reported to present osteoconductivity and the ability to enhance bone formation, both, *in vivo* and *in vitro*.[14] CTS can also be utilized for the controlled release of pharmacological agents and has been shown to be an effective nonviral vector for gene delivery.[13–16]

The use of CTS to modify PHB properties has been reported. An improvement of the brittle behavior of PHB in devices has been reported by Ikejima et al.,[12] who produced films of PHB/CTS by casting using 1,1,1,3,3,3-hexafluoro-2-propanol (HFIP) as a solvent. Moreover, Peschel et al.[17] produced porous PHB/CTS films mixing CTS dissolved in acetic acid with PHB in chloroform solution. The PHB/CTS films presented higher elongation at break than the pure PHB films and keratinocyte cell adhesion was also improved. Besides, CTS properties can also be improved by using PHB as reported by Cao et al.[18] who produced PHB/ CTS films using emulsion techniques. The authors claim that PHB/CTS films obtained presented lower elastic modulus, higher elongation-at break, higher tensile strength, and better cytocompatibility compared with pure CTS films. In a different approach, CTS can be employed as a modifying surface agent in 3D PHB scaffold, improving human osteoblasts adhesion.[19] All of these results encourage research on designed scaffolds made of PHB and CTS although few studies on 3D scaffolds made of PHB and CTS are found in literature.

The most common techniques for 3D-scaffold fabrication are particle leaching, gas foaming, emulsion freeze drying, electrospinning, rapid prototyping, and thermally induced phase separation, all of which require a polymer solution or polymer melting using a porogenic agent as the starting point.[20] In fact, there are few common solvents for CTS and aliphatic polyesters, and solvents such as HFIP and dimethyl sulfoxide are expensive and difficult to remove completely.[12,21] The use of PHB and CTS in the melting state, on the other hand, may be limited by the thermal behavior of CTS.[12] Studies have revealed that CTS tends to degrade before melting.[22]

In this article, a new and simple methodology is proposed to fabricate PHB/CTS 3D scaffolds. In this new technique, the capability of CTS to swell in aqueous solution was applied to form a 3D structure with open pores inside of a PHB 3D scaffold, which may be potentially applied in tissue engineering. Interconnected pores of different sizes and distributions were successfully obtained. One of the advantages of this technique is the production of scaffolds with both, bulk and surface, functionalized with CTS, which interacts with proteins such as fibronectin and induces HOB adhesion.[5,19] Generally, bulk and surface functionalization are desirable to achieve specific cell responses, and both can be realized after scaffold production.[23] However, bulk modification can affect the mechanical properties of the scaffolds. Moreover, this technique may be potentially employed using many different biological fluids that can render functionalized biomimetic 3-D structures and/or scaffolds with drug-delivery capabilities.

EXPERIMENTAL

Food-grade CTS with a 22% degree of acetylation was purchased from Polymar SA (Ceará, Brazil). PHB, in white powder form, with a molecular weight of (M_w) 524.000 g mol^{-1} was supplied by PHB Industrial S/A (São Paulo, Brazil). Both polymers were used as received.

Scaffolds Production

Scaffold production was carried out in three steps. In the first step, 10 g of a powder mixture of CTS and PHB with CTS percentage in the mixture equal to 2%, 5%, 10%, and 25% wt was added to 100 mL of chloroform:acetic acid 96 : 4 (v/v) solution. The mixture was heated to 60°C for 2 h under magnetic mixing, and the resulting solution 10% (w:v) was cast in glass molds and left to dry at room temperature for 72 h. The obtained specimens, from now on referred to as Pre-scaffold structures, were identified according to the CTS content in the primary mixture: Pre-S_{PHB} (0% wt of CTS), Pre-$S_{PHB\text{-}CTS2\%}$, Pre-$S_{PHB\text{-}CTS5\%}$, Pre-$S_{PHB\text{-}CTS10\%}$, and Pre-$S_{PHB\text{-}CTS25\%}$ (for 2%, 5%, 10%, and 25% wt of CTS, respectively). When reference is made to all concentrations of CTS, the Pre-scaffold will be denoted Pre-$S_{PHB\text{-}CTSx}$.

The second step was based on the capability of CTS molecules to swell in different fluids. In the present work, the Pre-scaffolds were swollen by immersion in water for 12 h and then frozen in liquid nitrogen. In the third step, the absorbed frozen fluid was removed by lyophilization to render porous structures. The obtained scaffolds were identified according to the CTS content in the primary mixture as $S_{PHB\text{-}CTSx}$, where x is 2%, 5%, 10%, or 25%. The scaffolds were repeatedly washed in distilled water until neutrality.

Characterization of the PHB/CTS Pre-Scaffolds and PHB/CTS 3D Scaffolds

Scanning Electron Microscopy (SEM). For cross-section analysis, the scaffolds were fractured in liquid nitrogen and coated with a thin layer of sputtered gold. The gold-coated samples were then observed in a scanning electron microscope (JEOL, JSM-6460 LV) operating at 10 kV.

X-ray Diffraction (XRD). XRD analyses were conducted using a diffratometer (Mini Flex II, Rigaku) operated with CuKα source ($\lambda = 1.542$ Å). The scan was recorded over the range of $2\theta = 6$–$60°$ at a scan speed of 2° s^{-1}. The XRD data were utilized to calculate the crystallinity degree (X_c) according to eq. (1).

$$X_c = A_c/A_t \quad (1)$$

where A_c is the area of the crystalline region and A_t is the total area under the diffractogram.

The XRD data were also used to calculate the apparent crystallite size (t) according to Sherrer's formula [eq. (2)].[24]

$$t = 0.9\lambda/(B\cos\theta) \quad (2)$$

where t is apparent crystallite size, λ is the X-ray wavelength and B is the full width at the half maximum and θ is the angle, in radians, at which the intensity is maximum.[24] For this calculation, a diffraction peak corresponding to the plane hkl (020) was used.

Differential Scanning Calorimetry (DSC). The PHB, CTS and the Pre-$S_{PHB\text{-}CTSx}$ were heated to 200°C and then cooled to –20°C. Then, the samples were heated to 210°C at a heating rate 10°C min^{-1}, and DSC curves were recorded.

Fourier-Transformed Infrared Spectroscopy (FTIR). A chemical analysis of all scaffolds was carried out using an FTIR (Perkin-Elmer 1720X) spectrophotometer under attenuated total reflectance by recording measurements from 4500 to 600 cm^{-1}.

Swelling Degree. The swelling degree (S_w) of the Pre-$S_{PHB\text{-}CTSx}$ produced in the second step was determined by immersing the Pre-$S_{PHB\text{-}CTSx}$ in distilled water for 12 h and measuring the weight variation (W_t) relative to the initial weight (W_0) in intervals of 2 h. The degree of swelling is calculated using eq. (3).

$$S_w(\%) = [(Wt - W_0)/W_0] \times 100 \quad (3)$$

Swelling Dimensionality Index. The swelling dimensionality index (d) allows to analyze the swelling behavior. To obtain d values the Pre-scaffold (cylindrical shape) were swollen in distilled water and the diameter (D) and height (h) of swollen scaffolds at different times (0, 2, 4, 6, 8, 10, and 12 h) were measured. From these data scaffolds volume and area were obtained by eqs. (4) and (5) respectively. The d value was obtained based on the methodology by Peppas et al.[25] where d value can be obtained plotting the ln[Agel/Adry] (where Agel is

Applied Polymer SCIENCE

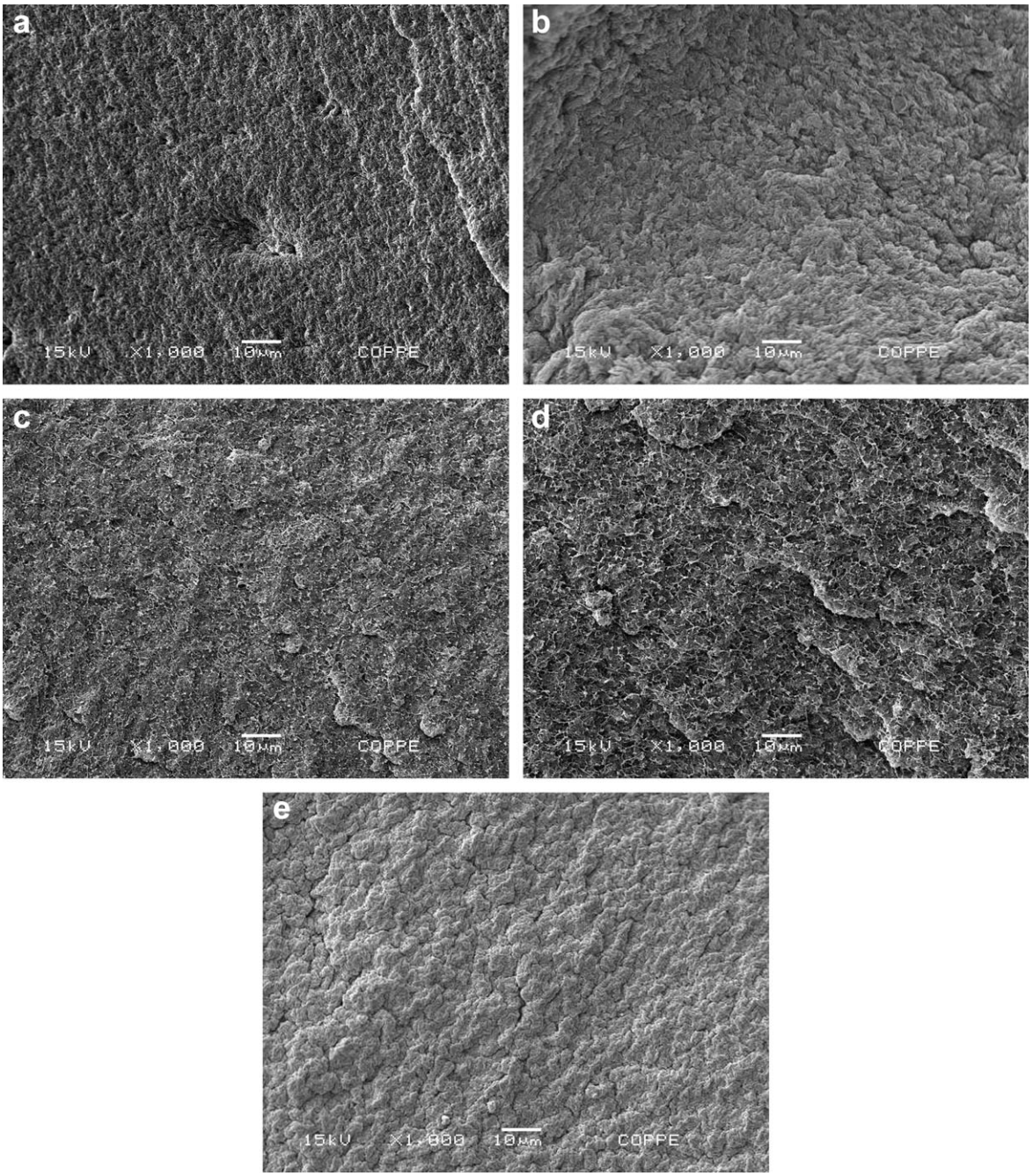

Figure 1. SEM images of cross section surface of the dense matrix of PHB and CTS named as Pre-scaffolds obtained in the first step of scaffold production: (a) S_{PHB}, (b) Pre-$S_{PHBCTS2\%}$, (c) Pre-$S_{PHBCTS5\%}$, (d) Pre-$S_{PHBCTS10\%}$, and (e) Pre-$S_{PHBCTS25\%}$. Note that no pores were formed in this step.

the area of swollen sample and Adry is the area of the dry sample) versus the ratio between swollen sample volume and dry sample volume (Q) where the slope is (d-1)/3.

$$A = \pi.(D^2/2 + D.h) \quad (4)$$

where A is the scaffold area and π is approximately 3.14.

$$V = \pi.h.D^2/4 \quad (5)$$

where V is the scaffold volume

Scaffolds Porosity. The porosity was determined by measuring the ratio of the pore (void) volume to the apparent (total) volume of a porous material, as described by ASTM D 4404 (Liquid Intrusion technique). The porosity was calculated according to eq. (6).

$$\text{Porosity} = 100 \times V_P/V_T \quad (6)$$

where V_p is the pore volume, V_T is the total volume.

The pores volume was calculated according to eq. (7).

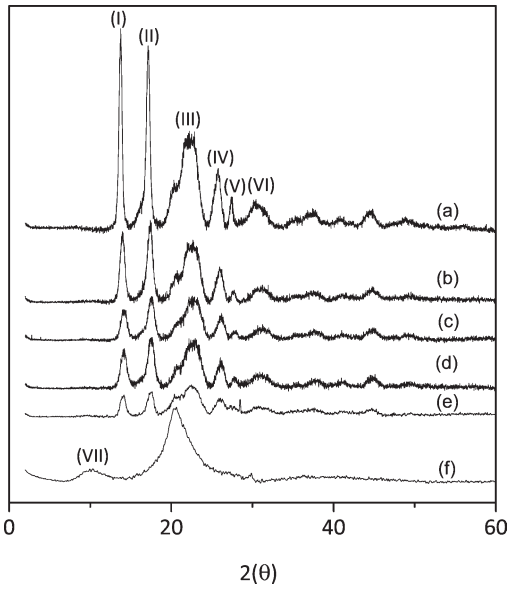

Figure 2. X-ray diffractograms of (a) S_{PHB}, (b) Pre-$S_{PHBCTS2\%}$, (c) Pre-$S_{PHBCTS5\%}$, (d) Pre-$S_{PHBCTS10\%}$, (e) Pre-$S_{PHBCTS25\%}$, and (f) CTS. The spectra for all Pre-$S_{PHBCTSx}$ were obtained in the first step of scaffold production. The spectra are vertically translated for better clarity.

$$V_P = V_T - \mathrm{ms/s} \quad (7)$$

where ms is the scaffold weight and ρs is the scaffold density. The scaffold density was obtained as the ratio between the scaffold weight and external volume (obtained by determining the scaffold diameter and height, assuming that a cylindrical scaffold was constructed).

***In Vitro* Degradation.** Local inflammation due to biomaterial implantation leads to an acidic pH. To mimic this pH and evaluate the scaffold degradation, the 3D structures were immersed in acetate buffer solution (1.0*M* pH 5.0) at 37°C and the degradation was evaluated in intervals of 10 days until a total of 3 months. The degraded scaffolds were analyzed by SEM.

Compressive Tensile Behavior. The compressive tensile strength of the samples was measured using a universal testing machine (Instron 5567) with a 2 KN cell and crosshead speed of 1.3 mm min^{-1}. The samples measured approximately 12 mm in diameter and 3.6 mm in height.

Cytotoxicity Assays. The scaffolds were submitted to cytotoxicity assays according to the methodology described by De-Deus et al.[26] The cells [murine osteoblasts (MC3T3)], were exposed to extract media (produced after incubating the scaffolds in culture medium for 24 h at 37°C in 5% CO_2 atmosphere) for 24 h, and the cytotoxicity was evaluated using a commercial kit (Cytotox, Xenometrix). This kit allows for the analysis of three different cell survival and integrity parameters: one based on the ability of mitochondrial dehydrogenase enzymes to convert the yellow water-soluble tetrazolium salt (XTT) to orange-colored soluble compounds of formazan, measured by their absorbance at 480 nm named as XTT; neutral red (NR) is a survival/viability test based on the ability of living cells to incorporate the NR dye in their lysosomes, where it accumulates in membrane-intact cells. The amount of dye incorporated can be measured at 540 nm. The other parameter is crystal violet dye elution (CVDE), which is a simple assay that evaluates cell density by staining DNA; after the elimination of excess dye, the absorbance at 540 nm is proportional to the amount of cells in the well. The absorbance was measured with a microplate UV/Vis spectrophotometer (Synergy 2, BioTek Instruments). A 2% phenol solution was used as positive control (cytotoxic) and a polystyrene extract, in the cell control only culture medium (Alpha MEM), was used as negative control (no cytotoxic).

RESULTS AND DISCUSSION

This new method of producing 3D scaffolds of PHB/CTS is predominantly based on the success of the Pre-$S_{PHB\text{-}CTSx}$ structure. To obtain a homogeneous and adequate pore size and pore-size distribution, CTS must be homogeneously dispersed in the PHB matrix. The proper swelling and removal of water is also essential to form interconnected open pores with controlled size. Therefore, a very well-controlled procedure in each step is mandatory to achieve the desired structure. Scaffold production was carried out in three steps: Pre-$S_{PHB\text{-}CTSx}$ formation, Pre-$S_{PHB\text{-}CTSx}$ swelling, and lyophilization. For close control over the process, the samples were characterized in all steps to evaluate the effect of CTS on pore formation and on the PHB properties in each stage. SEM images of the fracture surface of Pre-S_{PHB} (without CTS) and Pre-$S_{PHB\text{-}CTSx}$ produced in the first step are shown in Figure 1. All Pre-$S_{PHB\text{-}CTSx}$ presented a morphology that was distinct among all samples and from that observed for Pre-S_{PHB}. Pre-S_{PHB} presented the smoothest fracture surface. Rounded surface features were observed on the Pre-$S_{PHB\text{-}CTSx}$ surface as the amount of CTS in the scaffolds increased. It is worth noting that no pores were observed on any of the Pre-scaffold surfaces.

According to the literature, CTS can affect the crystallization behavior of PHB[12,27]; therefore, all the Pre-$S_{PHB\text{-}CTSx}$, PHB, and CTS were evaluated by XRD analysis. The obtained diffractograms are shown in Figure 2.

The main PHB peaks, labeled I to VI in Figure 2(a), occur at 2θ equal to 13.76°, 17.0°, 22°, 25.5°, 27.35°, and 30°. These peaks are related to the crystallographic plans (020), (110), (021) (111), (121), and (040), respectively.[28] The characteristic peaks of PHB are present in all of the Pre-$S_{PHB\text{-}CTSx}$ diffractograms, although changes in intensity and position can be observed. The intensity of peak I is reduced relative to that of peak II with the increase in CTS content. Moreover, peak V also decreases with the increase in the CTS content and practically disappears at 25% CTS. The peak at $2\theta = 20°$ is probably overlapped with PHB peak III. The results suggest that, indeed, the presence of CTS affects PHB crystallization.

The degree of crystallinity of the Pre-$S_{PHB\text{-}CTSx}$ was evaluated by XRD [eq. (1)]. The results are shown in Table I, which indicates an increase in the amount of CTS results in a decrease in the degree of crystallinity; therefore, all Pre-$S_{PHB\text{-}CTSx}$ are less crystalline than the pure PHB. This result is particularly important for the Pre-$S_{PHBCTS25\%}$, for which a substantial reduction was

Table I. Crystallinity Degree (X_c) and the Apparent Crystallites Sizes (t) Obtained by XRD Analysis

Sample	X_c (%)	t (Å) Plan (002)
S_{PHB}	50	174.1
$S_{PHB\text{-}CTS2\%}$	46	91.0
$S_{PHB\text{-}CTS5\%}$	49	116.1
$S_{PHB\text{-}CTS10\%}$	48	88.0
$S_{PHB\text{-}CTS25\%}$	35	102.7
CTS	46	174.1

observed, indicating that the amount of CTS affects the crystallization mechanism. The apparent crystallite sizes (t), calculated using eq. (2), related to the crystallographic plan 020 are shown in Table I. The apparent crystallite size decreases with the CTS content.

According to the literature, devices made of PHB and CTS have crystalline characteristics associated with both materials. Moreover, the resulting crystallinity may be affected not only by the amount of CTS but also by the methodology employed in device production.[13] The changes in the crystalline degree of the fabricated Pre-$S_{PHB\text{-}CTSx}$ suggest a strong interaction between CTS and PHB at the molecular level. Ikejima et al.[12] studied the crystalline properties of PHB/CTS films and attribute the decrease in the crystalline degree to the intermolecular interaction between CTS molecules surrounding PHB that would make the molecules less flexible, therefore hindering the formation of crystalline structures. This observation may be supported by considering the sizes of the Pre-$S_{PHB\text{-}CTSx}$ crystallites. According to Table I, the thickness (t) of the Pre-$S_{PHB\text{-}CTSx}$ crystals was smaller than that of the Pre-S_{PHB} crystals.

Table II. DSC Results of Pre-scaffolds Produced in the Third Step I

Sample	T_c (°C)	T_m (°C)	ΔH_c (J/g)	ΔH_f (J/g)
PHB	40.8	173.5	-30.63	56.69
Pre-$S_{PHBCTS2\%}$	51.5	158.49	-43.97	66.7
Pre-$S_{PHBCTS5\%}$	40.84	151.5	-40.84	59.77
Pre-$S_{PHBCTS10\%}$	46.37	153.36	-38.34	47.09
Pre-$S_{PHBCTS25\%}$	47.58	154.42	-17.11	23.96

The scaffolds were also evaluated by DSC, and the results related to the second heating are shown in Table II. All Pre-$S_{PHB\text{-}CTSx}$ presented similar melting temperatures, which were slightly reduced compared with the melting temperature of pure PHB. A decrease in ΔH_f was also observed for the Pre-$S_{PHB\text{-}CTSx}$. This result may indicate that thinner lamellar crystals of PHB were produced in the presence of CTS as a result of the intermolecular interaction between the polymers, corroborating the results from XRD shown in Table I.

It should be mentioned, however, that PHB is a very brittle material, and weak mechanical properties is one of the main drawbacks of fabricating PHB-based cell-support devices. As it is well documented in the literature, the brittleness of PHB is associated with its high crystallinity.[12] Therefore, the resulting reduction is a very positive result and can lead to an improvement in the mechanical properties of PHB.

CTS macromolecules have amino and hydroxyl groups available to form hydrogen bonds with molecules that have carbonyl groups, such as PHB.[12,27,29] The possible intermolecular interaction between CTS and PHB was evaluated by FTIR analysis of all Pre-$S_{PHB\text{-}CTSx}$ immediately after the first step of the fabrication process; the spectra are shown in Figure 3(b–e). For

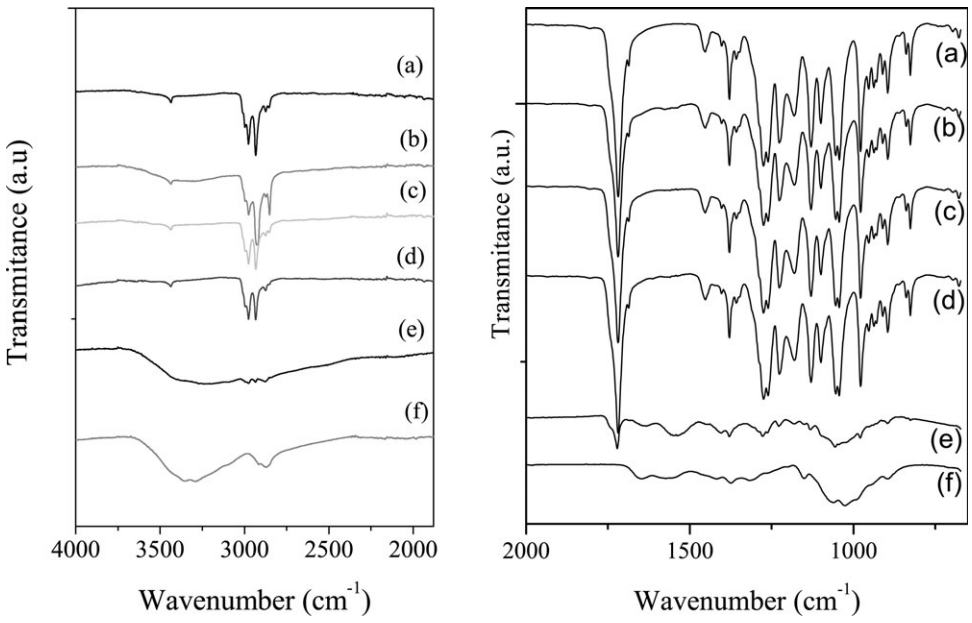

Figure 3. FTIR spectra of (a) S_{PHB}, (b) Pre-$S_{PHBCTS2\%}$, (c) Pre-$S_{PHBCTS5\%}$, (d) Pre-$S_{PHBCTS10\%}$, (e) Pre-$S_{PHBCTS25\%}$, and (f) CTS. I — Detail of 3650 cm^{-1} to 2500 m^{-1} and II detail of 1800 cm^{-1} to 1300 cm^{-1}).

comparison, the same figure shows the spectra of pure PHB and CTS, curves a and f, respectively. The characteristic C—H and C—C bands of PHB can be observed at about 2900 cm^{-1}.[30] The characteristic CTS bands at 3354 cm^{-1} and 3291 cm^{-1} are related to hydroxyl and amino groups, respectively, and appear to be overlapped in the spectra. The figure shows that the Pre-$S_{PHB\text{-}CTSx}$ spectra [Figure 3(b–e)] present the characteristic bands of both pure PHB and pure CTS. Moreover, the intensity of the CTS bands at 3354 cm^{-1} and 3291 cm^{-1} in the Pre-$S_{PHBCTSX}$ spectra increase with the CTS concentration. The Pre-S_{PHB}, Pre-$S_{PHBCTS2\%}$, Pre-$S_{PHBCTS5\%}$, and Pre-$S_{PHB\text{-}CTS10\%}$ also show a band at 3580 cm^{-1} attributed to the residual acetic acid that remains in the Pre-$S_{PHBCTSX}$ after the first step.[31] The stronger CTS band probably overlaps this peak in the Pre-$S_{PHBCTS25\%}$. Furthermore, with respect to the Pre-$S_{PHBCTS25\%}$, the effect of CTS content is much more noticeable than that in the other Pre-$S_{PHBCTSX}$, as can be observed in the spectra in Figure 3(e).

The band related to the CTS amino group occurs at about 1650 cm^{-1}.[27] However, the shift to lower wavenumbers indicates that hydrogen bonds are formed (see detail II in Figure 3 from 2000 cm^{-1} to 1450 cm^{-1}). In this region, the characteristic CTS bands are C=O in amide groups (amide I band) at approximately 1646 cm^{-1} and an NH_2 vibration band at about 1593 cm^{-1}; it can be observed in Figure 3 that only the Pre-$S_{PHBCTS25\%}$ presented characteristic CTS bands, although the amino group bands were observed to occur at lower wave numbers than the amino group bands of pure CTS.[22] This shift suggests hydrogen-bond formation between PHB and CTS, as also reported by Chen et al.,[21] who studied blends of PHB and CTS. Moreover, the increase in CTS content shifted the characteristic PHB band at 1720 cm^{-1} attributed to C=O vibration. This decrease can be attributed to changes in PHB crystallinity identified by XRD analysis.[12]

The capability of CTS to swell in the presence of water or biological fluids is well known and has been explored by some research groups studying hydrogels.[15,29] CTS physical hydrogels are formed by reversible links originating from secondary interactions, such as anionic, polyelectrolyte or secondary interaction complexes, grafted CTS hydrogels or simply entanglement. The latter can be formed simply by the solubilization of CTS in an acidic aqueous medium, which is the simplest way to prepare a CTS hydrogel.[32] In this work, because the process of swelling the Pre-$S_{PHB\text{-}CTSx}$ was carried out in acidic medium once acetic acid was employed during the first step of the fabrication process and was not neutralized, it is believed that a CTS hydrogel structure was formed. During the second step, the Pre-$S_{PHB\text{-}CTSx}$ were immersed in distilled water to promote CTS swelling and, consequently, physical and entangled CTS hydrogel formation in the PHB matrix. The swelling degree (S_w) of the Pre-$S_{PHB\text{-}CTSx}$ was calculated using eq. (3), and the S_w values for Pre-$S_{PHB\text{-}CTS2\%}$, Pre-$S_{PHB\text{-}CTS5\%}$, Pre-$S_{PHB\text{-}CTS10\%}$, and Pre-$S_{PHB\text{-}CTS25\%}$ were 51.5%, 48.6%, 53.1%, and 203% respectively. The S_w values can be related to the CTS content and distribution in the PHB matrix. For the scaffolds with 2–10% CTS, PHB can act as a barrier to water diffusion, thus hindering the swelling process. At those concentrations, CTS might interact with PHB molecules, and despite the variation in percentage, small changes in S_w for Pre-$S_{PHB\text{-}CTS2\%}$, Pre-$S_{PHB\text{-}CTS5\%}$, and Pre-$S_{PHB\text{-}CTS10\%}$ were observed. When 25% CTS was employed, the PHB barrier effect was minimized, both by a volume effect, through which CTS was better dispersed in the matrix, and a decrease in the PHB crystallinity degree, as observed by XRD.

The third step was carried out by lyophilization of the frozen, swollen Pre-$S_{PHB\text{-}CTSx}$ to remove the water. To investigate the process of pore formation after the lyophilization of the swollen material, the $S_{PHB\text{-}CTSx}$ cross-section fractured surfaces were analyzed by SEM; the images are shown in Figure 4. A dense structure was observed in the S_{PHB} [Figure 4(a)]. On the other hand, pores were observed in all scaffolds containing CTS, indicating that pore formation occurs by the swelling of CTS and subsequent lyophilization. Consequently, the type and distribution of the pores is determined by the CTS concentration and distribution in the PHB matrix. Dense regions were formed in scaffolds with CTS concentrations lower than 25% [indicated by arrows in the Figure 4(b–d)], while the pores that formed on the $S_{PHB\text{-}CTS25\%}$ were more homogeneously distributed throughout the entire evaluated surface. Thus, it can be supposed that $S_{PHB\text{-}CTS25\%}$ presents a more suitable structure for cell growth and biological fluid exchange. Therefore, the subsequent characterizations were carried out only on supports containing 25% CTS.

The crystallinity of $S_{PHB\text{-}CTS25\%}$ and Pre-$_{SPHB\text{-}CTS25\%}$ was compared by the normalized XRD as shown in Figure 5. It can be observed that after the second and the third steps there was no difference in the diffraction patterns of the sample. However, a more amorphous structure was obtained, and although peaks can still be observed, their intensities were substantially modified. Because the swelling process of CTS forces the dense PHB structure to open, it is possible that this process modifies the XRD curve. The calculated X_c was 24%, in contrast with the 35% for the Pre-$_{SPHB\text{-}CTS25\%}$. This reduction in crystallinity may be associated with changes in intermolecular interactions between PHB and CTS due to the swelling of the structure (second step).

To investigate possible changes in intermolecular interactions, the $S_{PHB\text{-}CTS\ 25\%}$ was analyzed by FTIR, and the resulting spectrum is shown in Figure 6(d). The spectra for CTS [Figure 6(a)], PHB [Figure 6(b)] and Pre-$S_{PHB\text{-}CTS25\%}$ [Figure 6(c)] are also shown for comparison. Water molecules remain in the scaffold after lyophilization, as indicated by the increase in the intensity of the OH bands in the region between 4000 cm^{-1} and 3000 cm^{-1}. In the region ranging from 1700 cm^{-1} to 1500 cm^{-1}, bands different from those of the Pre-$S_{PHB\text{-}CTS25\%}$ and the pure PHB or CTS can be observed. The characteristic crystalline PHB bands centered at 1279 cm^{-1} and 1228 cm^{-1} were suppressed, corroborating the XRD analysis, which indicates a reduction in material crystallinity after the third step.[33] Figure 6(c) shows that the intensity of the characteristic CTS band attributed to secondary amide bonds at 1545 cm^{-1} increases.[34] On the other hand, the band attributed to the C=O bond of PHB centered at 1720 cm^{-1} in the Pre-$S_{PHB\text{-}CTS25\%}$ shifted toward 1646 cm^{-1} in the $S_{PHB\text{-}CTS25\%}$, which indicates that this

Applied Polymer SCIENCE

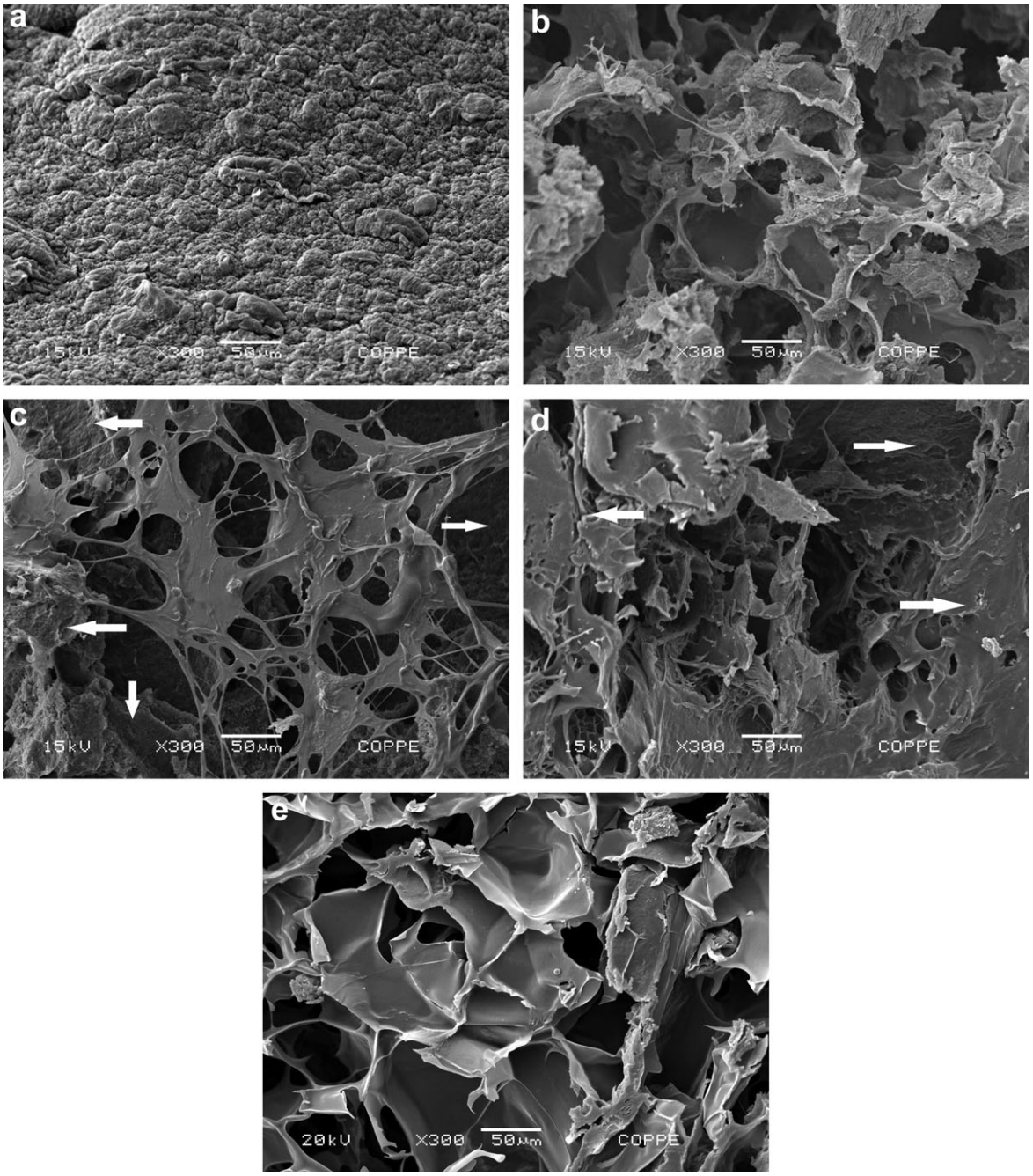

Figure 4. SEM images of the 3D scaffolds produced in the third step, obtained after the swollen and subsequently lyophilization of the Pre-scaffolds, (a) S_{PHB}, (b) $S_{PHBCTS2\%}$, (c) $S_{PHBCTS5\%}$, (d) $S_{PHBCTS10\%}$, and (e) $S_{PHBCTS25\%}$. Arrows indicate the dense regions.

group is probably involved in intermolecular interactions. The PHB band at 1720 cm^{-1} is also affected by crystallinity.[12] These results indicate that the CTS/PHB interaction in $S_{PHB\text{-}CTS25\%}$ is stronger than that in the Pre-$S_{PHB\text{-}CTS25\%}$.

Figure 7 shows the swelling kinetics of $S_{PHB\text{-}CTS\ 25\%}$. It was observed that the scaffold swelling increases approximately linearly until up to 10 h. Between 10 and 12 h a rapid increase is observed. Similar behavior was found by Khalid et al.[15] that investigated the swelling kinetics of CTS reference hydrogel, although a not so drastic increase in S_w between 10 and 12 h was observed. It is believed that, in this work, the PHB dense structure hampers water diffusion slowing down the swelling process. Once the water reaches the CTS structures, the swelling kinects is modified. The swelling dimensionality index (d) obtained for a total of 12 h of swelling was equal to 2.4. According to Peppas and Colombo[25] the d is an indicative of swelling anisotropy of the system and can be affected by the occurrence of restriction to the swelling. Typically d values between 2 and 2.5 are observed for slowly swelling or moderate hydrophilic system. PHB acts as restriction areas to swelling due

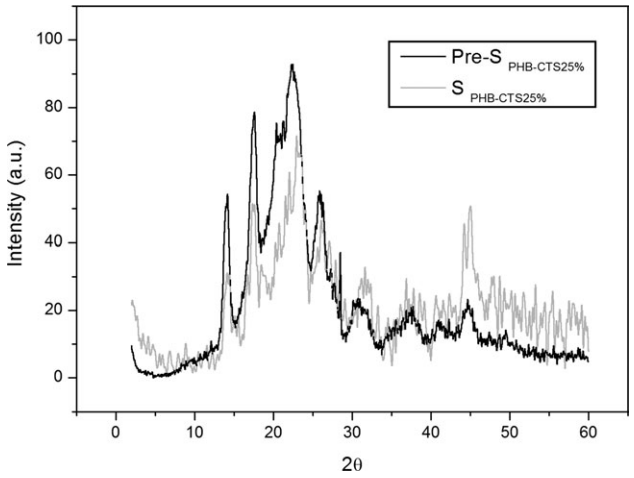

Figure 5. Normalized X-ray diffractogram of $S_{PHBCTS25\%}$ (darker line) and its precursor, Pre-$S_{PHBCTS25\%}$ (lighter line).

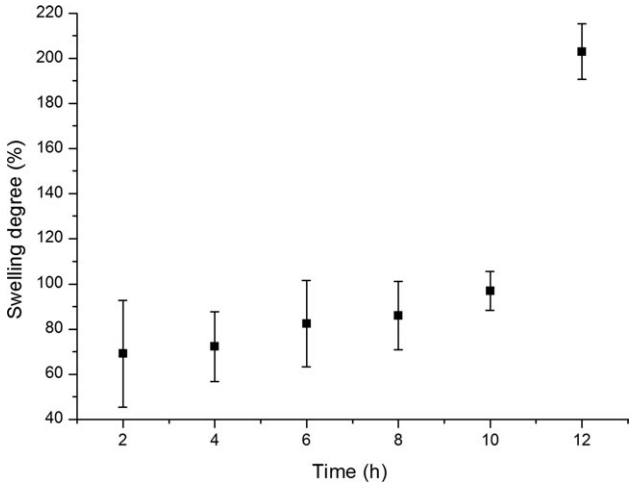

Figure 7. Swelling degree vs time for the Pre-$S_{PHBCTS25\%}$.

to its hydrophobic properties contrasting to the hydrophilic characteristics of CTS. This can justify the kinetics of the swelling during the analyzed period (Figure 7), where the highest S_w was obtained between 10 and 12 h. Pore formation of $S_{PHB\text{-}CTS25\%}$ as a function of the swelling time was evaluated by SEM; the images are shown in Figure 8. After 2 h of swelling, it is possible to note the initial swelling of CTS (indicated by arrows). The images suggest two process of pores formation. In the first process, as a result of CTS swelling, the PHB matrix that surrounds a CTS particle will open, and the second process results from the formation of CTS scaffold-like structures inside the PHB matrix [Figure 8(b)]. The arrow in Figure 8 indicates the PHB pore boundaries. It can be observed that different regions of the scaffold show different pore distributions and morphologies (see SEM images in Figure 9), which is related to the CTS distribution in the PHB matrix. The heterogeneous pore distribution may also be associated with the diffusion of water into the Pre-$S_{PHB\text{-}CTS25\%}$ and to the anisotropic swelling behavior. According to Hoffman,[35] a physical hydrogel is not homogeneous because clusters of molecular entanglements can create heterogeneities. In this study, physical gel-like structures

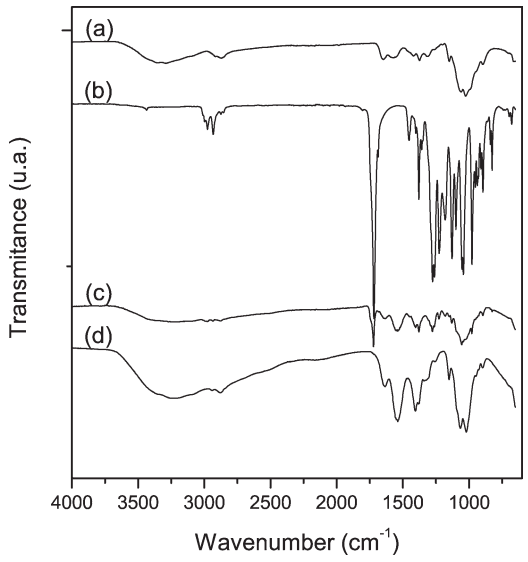

Figure 6. FTIR spectra of (a) Pure CTS, (b) pure PHB, (c) Pre-$S_{PHBCTS25\%}$, and (d) $S_{PHBCTS25\%}$.

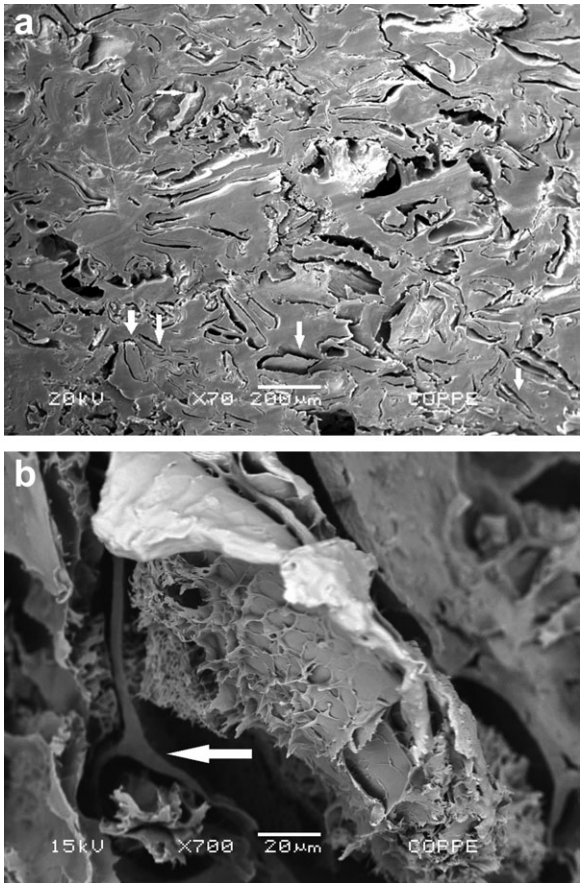

Figure 8. SEM images of $S_{PHBCTS25\%}$ for different swelling times: (a) 2 h — see CTS particles into the PHB matrix indicated by an arrow and (b) 6 h — see the PHB porous border indicated by the arrow and CTS 3D porous structure into the PHB porous.

Applied Polymer SCIENCE

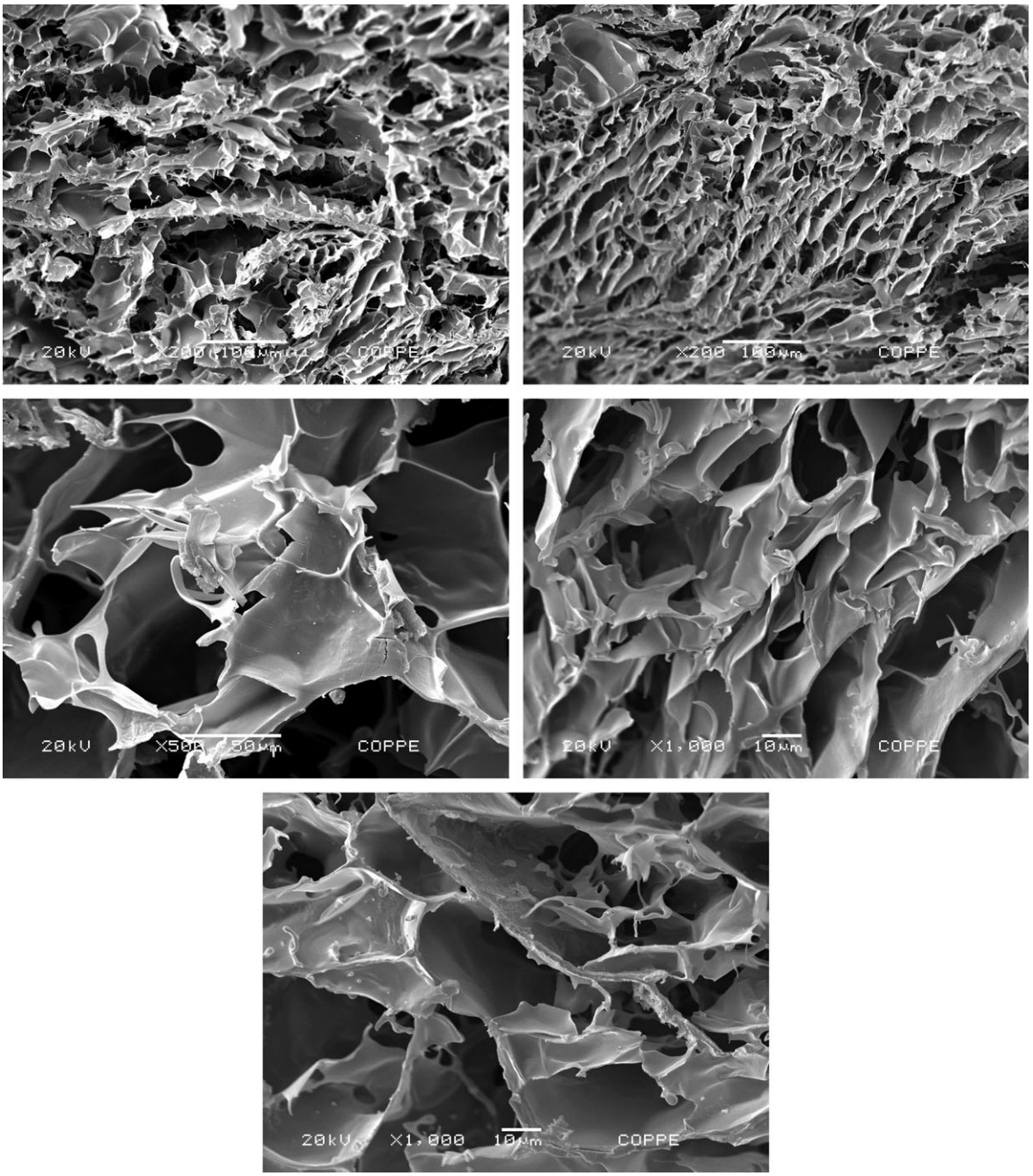

Figure 9. SEM images of different regions of the $S_{PHBCTS25\%}$ and porous size distribution of $S_{PHBCTS25\%}$ swelled by 12 h.

were probably produced in the second step and lyophilized in the third step, and once they were produced, they helped determine the scaffold structure. Indeed, the $S_{PHB\text{-}CTS25\%}$ showed regions with different porous sizes, morphologies, and orientations Figure 9).

The porosity of $S_{PHB\text{-}CTS25\%}$ was determined to be 70%. The pore-size distribution was determined by digital analysis of SEM images of the scaffold cross-section using Image Pro 6® (Figure 9). The scaffolds pore sizes and microscopic and macroscopic dimensions influence the cell behavior and are defined by the kind of cell and tissue to be regenerated because these factors affect the transport of nutrients and, consequently, tissue formation.[36] The optimum pore size depends on the application; indeed, different pore sizes are considered acceptable in bone-tissue engineering. According to Roosa et al.,[37] pores measuring 10–2250 μm have been used in bone-tissue engineering scaffolds, resulting in a varying degree of tissue ingrowth. The $S_{PHB\text{-}CTS25\%}$ presents a large pore-size window, although most of the pores are smaller than 50 μm. According to the literature, a pore size of 5 μm induces neovascularization, while sizes of 5–10 μm are related to fibroblast ingrowth.[38] Moreover, according to Santos et al.,[39] the growth of endothelial cells (the cell

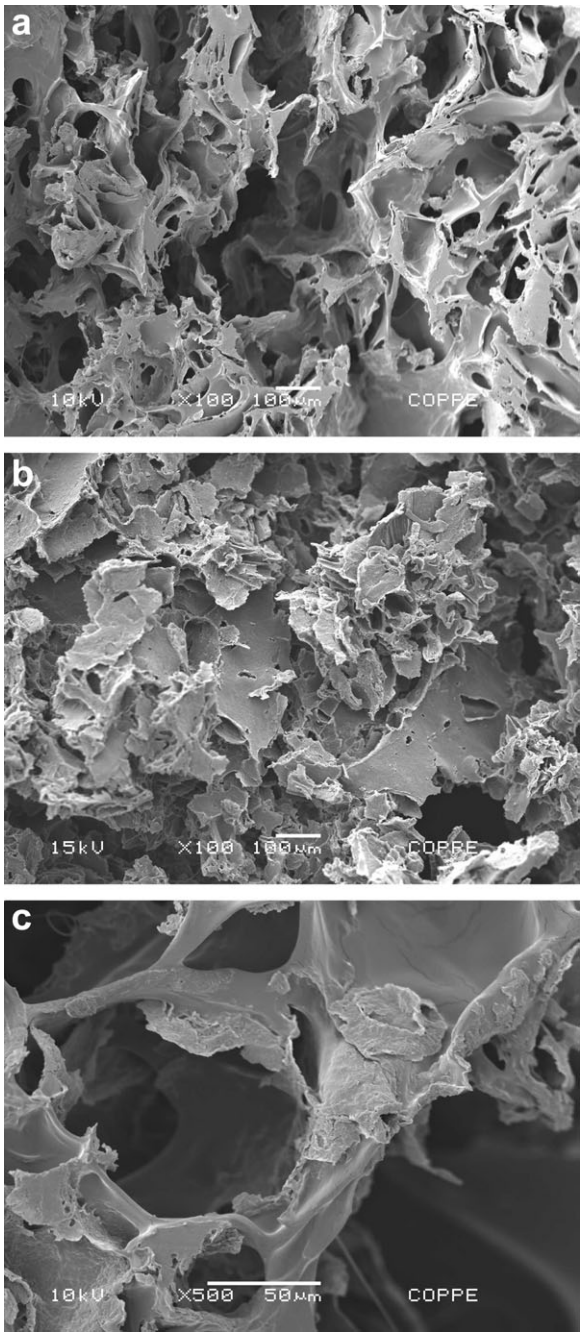

Figure 10. SEM images of $S_{PHBCTS25\%}$ degraded by (a) 10 days, (b) 3 months, (c) detail of (a) and (d) porous size distribution after 10 days of degradation in acetate buffer.

type that forms the inner lining of blood vessels) in 3D polymeric scaffolds is enhanced by smaller pores (5–20 μm) and smaller distances among neighboring pores. In bone-tissue engineering, pore sizes ranging from 100 to 400 μm induce bone regeneration and those ranging from 200 to 350 μm are suitable for osteoconduction, depending on the porosity and the materials used.[37] Given the obtained pore-size distribution, the $S_{PHB\text{-}CTS25\%}$ may initially seem best suited for neovascularization, although all the mentioned pore-size windows are present in the structure.

The scaffolds should have mechanical properties resembling those of healthy tissue during the period of tissue regeneration. The $S_{PHB\text{-}CTS25\%}$ was submitted to compressive mechanical testing, and the obtained compressive modulus was (13.07 ± 0.014) MPa. Bone is a complex tissue with different mechanical properties that depend on composition and structure.[40] Cortical bone exhibits compressive strengths ranging from 100 to 230 MPa, and cancellous exhibits compressive strengths ranging from 2 to 12 MPa.[41] The $S_{PHB\text{-}CTS25\%}$ has potential for application in the repair of cancellous bone. Mechanical properties are also affected by parameters such as porosity, composition, and material nature. The $S_{PHB\text{-}CTS25\%}$ presented a compressive modulus larger than some scaffold composites applied in bone-tissue engineering, with porosity values of about 70%, as in, for example, medical-grade polycaprolactone-tricalcium phosphate, which possesses a compressive modulus equal to 6.8 MPa.[41]

Degradation studies of $S_{PHB\text{-}CTS25\%}$, after 10 days [SEM images shown in Figure 10(a,b)] in acetate buffer at pH 5.0, showed that the CTS scaffolds formed in the PHB structure degrade

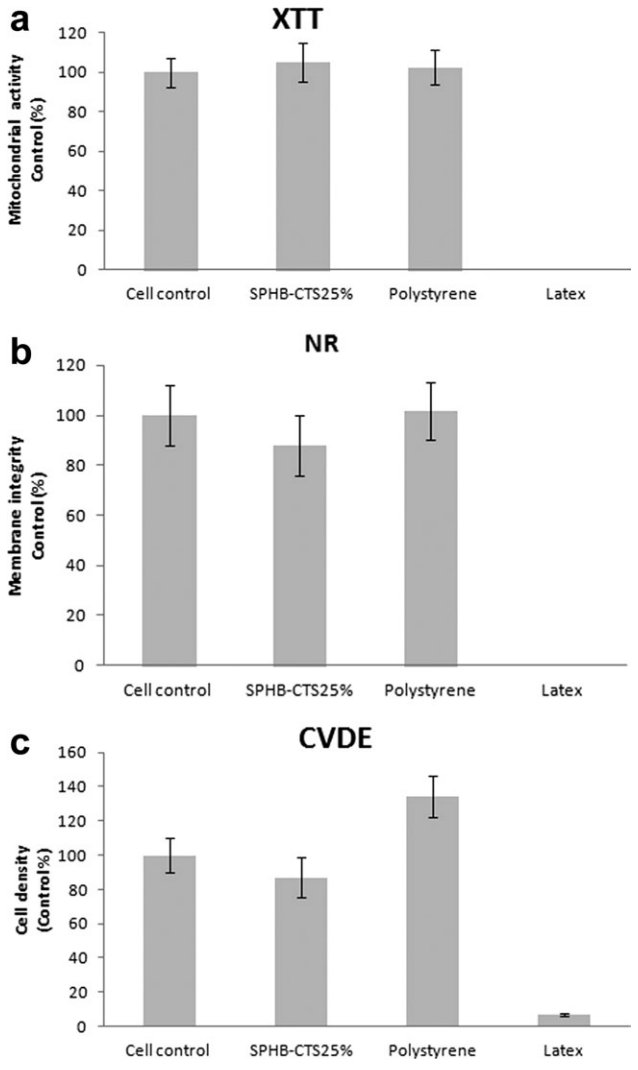

Figure 11. Graphic analysis of (a) cytotoxicity of respiratory activity, (b) NR, and (c) CVDE.

more quickly than the PHB porous structures, thus changing the pore-size distribution [Figure 10(c)] and forming open pores larger than the initial pores of the $S_{PHB\text{-}CTS25\%}$. Before degradation the biggest pores sizes was around 175 μm and after degradation was observed pore diameters of approximately 900 μm. This increase can be very advantageous to free space for nutrient transport and cell proliferation, and according to Roosa et al.,[39] the new pore-size distribution is adequate for bone formation. SEM images of $S_{PHB\text{-}CTS25\%}$ degraded after 3 months are shown in Figure 10(d); the images show very clear pore degradation. SEM images of pore formation in the scaffolds (Figure 8) indicate the presence of CTS particles in the PHB matrix. Thus, the Pre-$S_{PHB\text{-}CTS25\%}$ and consequently the $S_{PHB\text{-}CTS25\%}$ were formed by a biphasic amphiphilic system in which CTS is the hydrophilic component and PHB is the hydrophobic component. According to the literature, PHB has a high hydrolytic stability and takes several months to degrade in buffer solution.[42] CTS hydrolytic degradation occurs by the hydrolysis of amino bonds. Gupta et al.[43] evaluated the degradation of CTS microspheres in acid medium and reported that the spheres started to disintegrate after the 8th day. Thus, the degradation result obtained in the present work is in agreement with the results of the literature.

The scaffolds were submitted to multiparametric assays to evaluate their cytotoxicity behavior, and the results are shown in Figure 11. This combined method increases the probability of detection of a cytotoxic effect, since these dyes measure cell viability by different mechanisms: mitochondrial dehydrogenase activity (XTT), integrity of membrane of viable cells (NR), and DNA molecules stain (CV).[44] The XTT analyses [Figure 11(a)] showed no significant change in the cells' respiratory activity in comparison with the negative control (no cytotoxic). As expected, the positive control (2% phenol) impaired XTT mitochondrial activity. The NR analyses conducted to evaluate the cell survival/viability [Figure 11(b)]. It showed that the scaffolds presented no cytotoxicity behavior because no significant differences were observed between the cell control, the negative control and the $S_{PHB\text{-}CTS25\%}$. Phenol hampered the absorption of this dye. According to CVDE analysis [Figure 11(c)], cell viability was significantly reduced after exposure to phenol solution. However, the cell density was neither affected by extract media from the $S_{PHB\text{-}CTS25\%}$ nor from the negative control. The XTT, NR and CVDE results showed that the $S_{PHB\text{-}CTS25\%}$ was not cytotoxic.

CONCLUSIONS

PHB/CTS porous 3D scaffolds were successfully prepared using a new methodology based on the swelling behavior of CTS. The amount of pores in the PHB matrix was a function of the CTS content distribution in the Pre-scaffolds. CTS content 25% was the percentage where a significant reduction on the crystallinity was observed (which contributed to improve PHB mechanicals properties). Besides, for the Pre-scaffold with CTS content equal to 25% the barrier effect of PHB was minimized and the swelling properties of CTS were highly promoted, which contributed to the creation of the desired porogenic structure. The pore-size distribution was affected by the degradation, and it was observed that the CTS scaffolds inside the PHB pores tend to degrade at different rates.

ACKNOWLEDGEMENTS

The authors thank CNPq for their financial support, PHB Industrial S/A for the PHB supply and Unidade de Pesquisa Clínica do Hospital Antônio Pedro/UFF, Brazil for cytotoxicity analysis.

REFERENCES

1. Orlando, G.; Wood, K. J.; Stratta, R. J.; Yoo, J. J.; Atala, A.; Soker, S. *Transplantation* **2011**, *91*, 1310.
2. Stevens, M. M. *Mater. Today* **2008**, *11*, 18.
3. Olson, J. L.; Atala, A.; Yoo, J. J. *Chonnam Med. J.* **2011**, *47*, 1.
4. Hutmacher, D. *Biomaterials* **2000**, *21*, 2529.
5. Gomes, S.; Leonor, I. B.; Mano, J. F.; Reis, R. L.;. Kaplan, D. L. *Prog. Polym. Sci.* **2012**, *37*, 1.
6. Patterson, J.; Martino, M.; Hubbell, J. A. *Mater. Today* **2010**, *13*, 2.
7. Fillipczakk, K.; Janik, I.; Kozicki, M.; Ulanski, P.; Rosiak, J. M.; Pajewski, L. A.; Olkowski, R. M.; Wozniak, P.; Chróścicka, A.; Lewandowska-Szumieł, M. *E-Polymers* **2005**, *20*, art 11.
8. Thiré, R. M. S. M.; Mendonça, R. H.; Silva Filho, F. C.; Costa, M. F. PHB Scaffolds Modified with Chitosan and Fibronectin to Improve HOB Adhesion, In: Proceedings of 8th World Biomaterials Congress, Amsterdan, **2008**.
9. Thiré, R. M. S. M.; Meiga, T. O.; Dick, S.; Andrade, L. R. *Macromol. Symp.* **2007**, *258*, 38.
10. Sudesh, K.; Abe, H.; Doi, Y. *Prog. Polym. Sci.* **2000**, *25*, 1503.
11. Sader, M. S.; Ferreira, M.; Dias, M. L. *Polímeros* **2006**, *16*, 12.
12. Ikejima, T.; Yagi, K.; Inoue, Y. *Macromol. Chem. Phys.* **1999**, *200*, 413.
13. Shih, W-J.; Chen, Y-H.; Shih C-J.; Hon, M-H.; Wang, M-C. *J. Alloys and Compds.* **2007**, 434–435, 826.
14. Martino, A. D.; Sittinger, M.; Risbud, M. V. *Biomaterials* **2005**, *26*, 5983.
15. Khalid, M. N.; Agnely, F.; Yagoubi, N.; Grossiord, J. L.; Couarraze, G. *J. Pharm. Sci.* **2002**, *15*, 425.
16. Nettles, D. L.; Steven, M. S.; Elder, H.; Gilbert, J. A. *Polímero: Ciência e Tecnologia* **2002**, *6*, 1009.
17. Peschel, G.; Dahse, H. M.; Konrad, A. *J. Biomed. Mater. Res. Part B* **2008**, *85A*, 1072.
18. Cao, W.; Wang, A.; Jing, D.; Gong, Y.; Zhao, N.; Zhang, X. *J. Biomater. Sci. Polym. Ed.* **2005**, *16*, 1379.
19. Mendonça, R. H.; Thiré, R. M. S. M.; Costa, M. F.; Silva Filho, F. C. In: 5° Congresso Latino Americano de Órgãos Artificiais e Biomateriais, 2008, Ouro Preto. CD dos Anais do 5° COLAOB, **2008**.
20. Tsang, V. L.; Bathia, S. N. *Adv. Drug Delivery Rev.* **2004**, *56*, 1635.

21. Chen, C.; Zhou, X.; Zhuang, Y.; Dong, L. *J. Polym. Sci. Part B: Polym. Phys.* **2005**, *43*, 35.
22. López, F. A.; Merc A. L. R.; Alguacil, F. J.; López-Delgado, E. *J. Therm. Anal. Calorim.* **2008**, *91*, 633.
23. Ma, P. X. *Adv. Drug Delivery Rev.* **2008**, *60*, 184.
24. Oliveira, S.; Araújo, E. S.; Guedes, S. M. L. *Polym. Degrad. Stabil.* **2006**, *91*, 2157.
25. Peppas, N. A.; Colombo, P. *J. Control. Release* **1997**, *45*, 35.
26. De-Deus, G.; Canabarro, A.; Alves, G.; Linhares, A.; Senne, M. I.; Granjeiro, J. M. *Basic Res. – Technol.* **2009**, *35*, 1387.
27. Chen, C.; Dong, L.; Cheung, M. K. *Eur. Polym. J.* **2005**, *41*, 958.
28. Skrbic, Z.; Divjakovic V. *Polymer* **1996**, *37*, 505.
29. Berger, J.; Reist, M.; Mayer, J. M.; Felt, O.; Gurny, R. *Eur. J. Pharmacol. Biopharm.* **2004**, *57*, 35.
30. Bloembergen, S.; Holden, D. A.; Hamer, G. K.; Bluhm, T. L.; Marchessault, R. H. *Macromolecules* **1986**, *19*, 2865.
31. Liao, L-F.; Lien, C-F.; Lin, J-L. *Phys. Chem. Chem. Phys.* **2001**, *3*, 3831.
32. Berger, J.; Reist, M.; Mayer, J. M.; Felt, O.; Peppas, N. A.; Gurny, R. *Eur. J. Pharmacol. Biopharm.* **2004**, *57*, 19.
33. Xu, J.; Guo, B-H.; Yang, R.; Wu, Q.; Chen, G-Q.; Zhang, Z-M. *Polymer* **2002**, *43*(25), 6893.
34. Altiok, D.; Altiok, E.; Tihminlioglu, F. *J. Mater. Sci.: Mater. Med.* **2010**, *21*, 2227.
35. Hoffman, A. S. *Adv. Drug Delivery Rev.* **2002**, *43*, 3.
36. Patel, Z. S.; Young, S.; Tabata, Y.; Jansen, J. A.; Wong, M. E. K.; Mikos, A. G. *Bone* **2008**, *43*, 931.
37. Roosa, S. M. M.; Kemppainen, J. M.; Moffitt, E. N.; Krebsbach, P. H.; Hollister, S. J. *J. Biomed. Mater. Res. Part A* **2010**, *92A*, 359.
38. Oh, S. H.; Park, I. K.; Kim, J. M.; Lee, J. H. *Biomaterials* **2007**, *28*, 1664.
39. Santos, M.; Reis, R. L. *Macromol. Biosci.* **2010**, *10*, 12.
40. Fratzl, P.; Weinkamer, R. *Prog. Mater. Sci.* **2007**, *52*, 1263.
41. Hutmacher, D. W.; Schantz, J. T.; Lam, C. X. F.; Tan, K. C.; Lim, T. C. *J. Tissue Eng. Regen. Med.* **2007**, *1*, 245.
42. Renard, E.; Walls, M.; Guérin, P.; Langlois, V. *Polym. Degrad. Stab.* **2004**, *85*, 779.
43. Gupta, K. C.; Kumar, M. N. V. *Biomaterials* **2000**, *21*, 1115.
44. Ishiyama, M.; Tominaga, H.; Shiga, M.; Sasamoto, K.; Okhura, Y.; Ueno, K. *Biol. Pharm. Bull.* **1996**, *19*, 1518.